Original Article

DOI: 10.5582/bst.2024.01360

N^5-((perfluorophenyl)amino)glutamine regulates BACE1, tau phosphorylation, synaptic function, and neuroinflammation in Alzheimer's disease models

Jun-Sik Kim[1,§], Yongeun Cho[1,§], Jeongmi Lee[1,§], Heewon Cho[1], Sukmin Han[2], Yeongyeong Lee[1], Yeji Jeon[1], Tai Kyoung Kim[3], Ju-Mi Hong[3], Jeonghyeong Im[1], Minshik Chae[1], Yujeong Lee[1], Hyunwook Kim[4], Sang Yoon Park[4], Sung Hyun Kim[2,5], Joung Han Yim[3,*], Dong-Gyu Jo[1,6,7,8,*]

[1] School of Pharmacy, Sungkyunkwan University, Suwon, Korea;
[2] Department of Neuroscience, Graduate School, Kyung Hee University, Seoul, Korea;
[3] Division of Polar Life Sciences, Korea Polar Research Institute, Incheon, Korea;
[4] Bio Research Dept, Ahngook Pharmaceutical Co., Gwacheon, Korea;
[5] Department of Physiology, School of Medicine, Kyung Hee University, Seoul, Korea;
[6] Samsung Advanced Institute for Health Sciences and Technology, Sungkyunkwan University, Seoul, Korea;
[7] Biomedical Institute for Convergence, Sungkyunkwan University, Suwon, Korea;
[8] Institute of Quantum Biophysics, Sungkyunkwan University, Suwon, Korea.

SUMMARY: Alzheimer's disease (AD) is the most common type of dementia. Its incidence is rising rapidly as the global population ages, leading to a significant social and economic burden. AD involves complex pathologies, including amyloid plaque accumulation, synaptic dysfunction, and neuroinflammation. This study explores the therapeutic potential of N^5-((perfluorophenyl)amino)glutamine (RA-PF), a derivative of γ-glutamyl-N'-(2-hydroxyphenyl)hydrazide (Ramalin), a compound with antioxidant and anti-inflammatory properties. Administration of RA-PF to 5xFAD mice decreases BACE1, reduces Aβ plaque deposition, inhibits microglial activation, restores synaptic transmission, and improves mitochondrial motility, leading to the recovery of cognitive function. Additionally, RA-PF treatment in 3xTg-AD mice alleviates anxiety-like behaviors, tau phosphorylation via inactivating GSK-3β, and BACE1 expression. Further transcriptomic analysis reveals RA-PF treatment in AD mice models recovers phagosome, inflammation, NOD-like receptor, presynaptic membrane, and postsynaptic membrane related signaling pathways. These findings suggest that RA-PF effectively targets multiple aspects of AD pathology, offering a novel multi-target approach for AD treatment.

Keywords: Alzheimer's disease (AD), ramalin, RA-PF, BACE1, tau, synaptic function

1. Introduction

Alzheimer's disease (AD) is a degenerative brain disorder and the most prevalent form of dementia (*1-3*). The pathological features of AD include the accumulation of β-amyloid (Aβ) and tau proteins, neuroinflammation, and neuronal death, leading to a reduction in brain volume that is directly related to memory impairment (*4-6*). Beta-site amyloid precursor protein cleaving enzyme 1 (BACE1) is a key player in the production of Aβ, which has been identified as a primary target for AD treatment (*7-11*). Neuroinflammation also plays a crucial role in the AD pathogenesis. Inflammatory responses accelerate AD progression, and they are activated even before the onset of symptoms (*12,13*). Inhibition of neuroinflammation has been reported to show pre-clinical results in preventing AD onset (*14,15*).

Here, we introduce γ-glutamyl-N'-(2-hydroxyphenyl) hydrazide (Ramalin) derivative showing pre-clinical efficacy on AD progression. Ramalin, isolated from the Antarctic lichen *Ramalina terebrata*, is known for its potent antioxidant, anti-inflammatory, and antibacterial effects (*16,17*). To enhance these therapeutic potentials, we designed and synthesized derivatives of ramalin by replacing its phenyl ring with various structural groups. From these derivatives, N^5-((perfluorophenyl)amino) glutamine (RA-PF) was identified through toxicity screening as exhibiting the lowest *in vivo* toxicity. And it is bioavailable and capable of penetrating the blood-brain barrier. In this study, we demonstrated RA-PF's

therapeutic effects on 5xFAD (*10,11*) and 3xTg-AD mice (*10,11*), which express mutations associated with familial AD (5xFAD: human APP (Swedish, Florida, London mutations) and PSEN1 (M146L and L286V mutations) and 3xTg: APP (Swedish), MAPT (P301L), and PSEN1 (M146V)). It reduces Aβ plaque deposition by regulating BACE1 expression, inhibits tau phosphorylation, restores hippocampal neuronal transmission, and ameliorates neuroinflammatory responses in AD models. These findings highlight the potential of ramalin derivative, RA-PF as a therapeutic strategy for AD.

2. Materials and Methods

2.1. Animals

This study used 3xTg-AD (B6;129-Tg(APPSwe, tauP301L)1Lfa *Psen1*^{tm1Mpm}/Mmjax) and 5xFAD (B6.Cg-Tg(APPSwFlLon,PSEN1*M146L*L286V)6799Vas/Mmjax) for AD animal models. All mice were kept in a 12-hour light/dark cycle with unrestricted access to food and water. 3xTg-AD mice were administered with 20 mg/kg of RA-PF once a day orally for 1.5 months and 5xFAD mice were treated with 20 mg/kg of RA-PF once a day orally for 2 months, respectively. After treatment, the mice underwent behavioral tests. All animal experimental procedures were approved by the Institutional Animal Care and Use Committee of Sungkyunkwan University (SKKUIACUC2022-10-41-1).

2.2. Synthesis method of RA-PF

Synthesis of benzyl N^2-((benzyloxy)carbonyl)-N^5-((perfluorophenyl)amino)glutaminate (p-Glu-PF-Hyd): A 250 mL round-bottom flask fitted with a magnetic stir bar was charged with (*S*)-5-(benzyloxy)-4-(((benzyloxy)carbonyl)amino)-5-oxopentanoic acid (2.0 g, 5.39 mmol) dissolved in 50 mL of dichloromethane (DCM). The reaction mixture was cooled to 0°C, and then triethylamine (TEA) (1.2 equivalents, 6.47 mmol, 902 µL) was added gradually. After 10 minutes, ethyl chloroformate (ECF) (1.2 equivalents, 6.47 mmol, 615 µL) was introduced dropwise over 1 hour. The mixture was stirred at 0°C for 4 hours. In a separate 100 mL pear-shaped flask, (perfluorophenyl)hydrazine (1.2 equivalents, 6.47 mmol, 1.28 g) was dissolved in 10 mL of DCM. This solution was then added slowly to the primary reaction flask over 1 hour while maintaining the temperature at 0°C. After the hydrazine was added, the reaction mixture was allowed to reach RT and stirred for an additional 16 hours. Upon completion, the organic layer was washed sequentially with distilled water, 1 N HCl, 0.5 N $NaHCO_3$, and distilled water again, before being separated and collected. The organic phase was dried over sodium sulfate (Na_2SO_4) and concentrated using a rotary evaporator. The target product was purified by recrystallization from a mixture of ethyl acetate and n-hexane (1:5). The synthesis yield of p-Glu-PF-Hyd is 92% (4.96 g).

Synthesis of N^5-((perfluorophenyl)amino)glutamine (RA-PF): A 500 mL round-bottom flask with a magnetic stir bar was loaded with the p-Glu-PF-Hyd (3.6 mmol, 2.0 g) and palladium on carbon (10 wt.%, 200 mg) in methanol (400 mL). The reaction mixture was stirred under hydrogen atmosphere (1 atm, using a hydrogen balloon) for 16 h. Once the reaction was complete, the mixture was passed through a 0.4 µm glass microfiber filter. The filtrate was then concentrated using a rotary evaporator, followed by purification through recrystallization from a 1:5 mixture of methanol and ethyl acetate. The synthesis yield of RA-PF is 80 % (940 mg).

2.3. Morris water maze

The Morris water maze test (MWM) was conducted to examine the spatial memory and learning abilities of the mice. The MWM was carried out as previously described with minor modifications (*18*). A pool with a diameter of 100 cm was used. Before the experiments began, the pool was filled with water to a level 1 cm higher than the platform, and non-toxic white pigment was added to prevent the mice from seeing the platform. The training sessions were conducted for 8 consecutive days, and mice were placed in three different locations each day. The escape latency and swimming speed were recorded by a camera. Each trial lasted for 60 seconds and if the mouse found the hidden platform within 60 seconds and stayed on it for 5 seconds, the mouse was returned to the cage. If the mouse did not find the platform within 60 seconds, it was put on the hidden platform and allowed to observe the surroundings for 10 seconds. All experimental data was recorded and analyzed by Ethovision software (Noldus).

2.4. Elevated plus maze test

The elevated plus maze test (EPM) is a widely used behavioral test to assess the anxiety of the mice (*19*). Briefly, the mouse was placed in the center of the elevated plus maze facing an open arm and allowed to explore for 5 minutes. Behavioral patterns were recorded and analyzed by Ethovision software (Noldus).

2.5. Brain tissue preparation

After behavioral tests, mice were sacrificed, and brain samples of mice were collected. Mice were anesthetized using Zoletil (Virbac) and Rompun (Bayer) and then perfused with phosphate-buffered saline (PBS). The two hemispheres of the brain were separated. One hemisphere was stored in 4% paraformaldehyde and the other was dissected into cortex and hippocampus. Dissected

samples were then snap-frozen in liquid nitrogen and stored at -80 ℃ until further analysis.

2.6. Microsomal stability assay

The metabolic stability of RA-PF was assessed using liver microsomes derived from humans and various animal species including mice, rats, dogs, and monkeys. This test was conducted by SPMED Co., Ltd (Republic of Korea). A 1 μM of RA-PF was incubated with liver microsomes at 37 ℃ for 30 minutes in the presence or absence of NADPH. The reaction was terminated by adding acetonitrile containing an internal standard. Samples were then centrifuged, and the supernatants were further analyzed by LC-MS/MS. The percentage of RA-PF remaining was calculated by comparing the quantified amount of RA-PF at 30 minutes to that at 0 minutes. This provided the % remaining value, which reflects the compound's metabolic stability under the test conditions.

2.7. Cytochrome P450 inhibitory assay

The inhibitory potential of RA-PF on key cytochrome P450 (CYP) isoforms (CYP1A2, CYP2C9, CYP2C19, CYP2D6, and CYP3A) was evaluated. This test was conducted by SPMED Co., Ltd (Republic of Korea). Human liver microsomes were incubated with phosphate buffer (pH 7.4), each CYP substrate (phenacetin for CYP1A2, diclofenac for CYP2C9, S-mephenytoin for CYP2C19, dextromethorphan for CYP2D6, and midazolam for CYP3A), and 10 μM of RA-PF in the presence of NADPH. The reaction was terminated by the addition of an acetonitrile containing an internal standard. Samples were then centrifuged, and the supernatant was analyzed by LC-MS/MS to quantify the amount of metabolites of each substrate drug.

2.8. Pharmacokinetic study

Pharmacokinetic parameters of RA-PF were measured using Sprague-Dawley rats by NeuroVis (Republic of Korea). Animals received 10 mg/kg of RA-PF *via* either oral administration or intravenous injection. Blood collection was performed using the BASi Culex ABS (Automated Blood Sampling) system. After catheter insertion into the jugular vein and carotid artery, the system was programmed to collect 200 μL blood samples at predetermined time points (0, 0.25, 0.5, 1, 2, and 7 hours). Blood samples were then centrifuged at 12,000 x rpm for 10 minutes, and the resulting plasma was immediately stored at -80 ℃. For brain pharmacokinetics analysis, 10 mg/kg of RA-PF was orally administered to Sprague-Dawley rats. Blood and brain tissue samples were collected post-administration. Samples were mixed with ofloxacin, an internal standard, and centrifuged at 13,000 x rpm for 5 minutes at 4 ℃. Supernatants were mixed with 50% methanol and analyzed by LC-MS/MS.

2.9. Mutagenicity assay (Ames test)

To evaluate whether RA-PF causes DNA mutation, the Ames test was performed using *Salmonella typhimurim* TA98, TA100, TA1535, TA1537 and *Escherichia coli* WP*2uvrA* (pKM101). 6 doses of RA-PF (50, 100, 500, 1,000, 2,500, and 5,000 μg/plate) were tested. RA-PF was incubated with S9 mix, each bacterial suspension, and top agar specific to each bacterium, followed by vortexing. The resulting suspensions were then overlaid onto minimum glucose agar plates, which were subsequently left at RT. After top agar solidified, plates were incubated at 37 ℃ for 48 hours. Following incubation, revertant colonies were then counted visually.

2.10. Cell culture

Human neuroblastoma cell line, SH-SY5Y, and mouse microglial cell line, BV-2 were maintained in DMEM (Hyclone) media supplemented with 10 % fetal bovine serum (Gibco) and 1 % penicillin/streptomycin (Capricorn) at 37 ℃ in a humidified atmosphere containing 5 % CO_2 (v/v). For the BV-2 cell line culture, heat-inactivated FBS was used. SH-SY5Y cells were treated with 5 μM and 10 μM of RA-PF for 24 hours. Then, cells were exposed to 200 μM of hydrogen peroxide (Sigma) for 2 hours. BV-2 cells were incubated with 5 μM and 10 μM of RA-PF for 24 hours and then treated with 0.1 μg/mL of lipopolysaccharide (Sigma) for 2 hours.

2.11. Primary neuron culture

Hippocampal CA1-CA3 regions were isolated from postnatal (0-3 day old) 5xFAD transgenic mice and plated on poly-ornithine-coated coverslips. Neurons were transfected 7 days after plating and further incubated for 14–21 days in a culture medium. All results are from at least three independent primary cultures. Animal treatments in this study were carried out in accordance with Animal Care and Use Guidelines, and all experiments were approved by the Animal Care Committee of Kyung Hee University (KHSASP-24-266).

2.12. *In vitro* optical imaging

For optical imaging, vGlut1-pHluorin(vG-pH) was transfected to primary cultured hippocampal neurons using the Ca^{2+} phosphate precipitation method, as previously described (*20*). Briefly, vG-pH was incubated with 2x HeBS (273 mM NaCl, 9.5 mM KCl, 1.4 mM $Na_2HPO_4 \cdot PO_2O$, 15 mM D-glucose, 42 mM HEPES, pH 7.10) containing 2 mM Ca^{2+}, subsequently, the mixture was applied to hippocampal neurons cultured for 8 days *in vitro* (DIV8). Live-cell imaging was conducted

on neurons at DIV14-21 neurons, which had been transfected with vG-pH 7 days post- plating. Neurons were present with 10 μM of RA-PF for 6 h. Coverslips containing neurons were mounted in a laminar-flow-perfused stimulation chamber on the stage of a custom-built, laser-illuminated epifluorescence microscope (Zeiss Observer). Live-cell images were captured using an Andor iXon Ultra 897 (Model #DU-897U-CS0-#BV) back-illuminated EMCCD camera. A diode-pumped OBIS 488 laser (Coherent) is used as the light source, with its TTL on/off synchronized with the EMCCD camera during image acquisition. Fluorescence excitation/emission and collection were performed using a 40 × Fluar Zeiss objective lens (1.3 NA) along with 500–550 nm emission and 498 nm dichroic filters (Chroma). Action potentials (APs) were induced by passing a 1-ms current pulse *via* platinum-iridium electrodes using an isolated current stimulator (World Precision Instruments). Neurons were perfused with Tyrode's buffer containing 119 mM NaCl, 2.5 mM KCl, 2 mM $CaCl_2$, 2 mM $MgCl_2$, 25 mM HEPES, 30 mM glucose, 10 μM 6-cyano-7-nitroquinoxaline-2,3-dione (CNQX), and D, L-2-amino-5-phosphonovaleric acid (AP5), with the pH adjusted to 7.4. All experiments were conducted at 30 ℃. All images were captured at 2 Hz with a 50-ms exposure.

2.13. *In vitro* imaging for mitochondria motility

For recording mitochondria motility, neurons were transfected with Mito-red plasmids at DIV7 and further incubated until 14-21 DIV. Live-cell imaging was carried out using a custom-built, laser-illuminated epifluorescence microscope (Zeiss Observer). Neurons expressing Mito-red were illuminated with a 561 nm laser and images were acquired every 3 seconds for 5 min. For analyzing mitochondria motility, the total number of Mito-red positive puncta were counted at the axon, and during the imaging period (5 min), more than 1 μm moving Mito-red is defined as motility of mitochondria.

2.14. Image analysis

All images were analyzed using Image J (http://rsb.info.nih.gov/ij) with the plugin Time Series Analyzer which is available at https://imagej.nih.gov/ij/plugins/time-series.html. Synaptic boutons were selected as oval regions of interest (diameter, 10 pixels), and the intensity of fluorescence at synapses was measured. Fluorescence traces were analyzed using Origin Pro (ver. 2020).

2.15. Western blot analysis

Cells were lysed with T-PER™ Tissue Protein Extraction Reagent (Thermo Scientific) supplemented with the protease/phosphatase inhibitor cocktail (Thermo Scientific) and incubated at 4℃ for 10 minutes. The samples were then centrifuged at 13,000 x rpm for 10 minutes at 4℃. The supernatant was used for western blot analysis. Mouse brain tissue samples were homogenized with RIPA lysis buffer (Merck) supplemented with the protease/phosphatase inhibitor cocktail. The homogenate was incubated at 4℃ for 20 minutes and the lysed samples were then centrifuged at 13,000×rpm for 20 minutes at 4℃. The supernatant was used for western blot analysis. Protein concentrations of lysed samples were quantified using Pierce™ BCA Protein Assay Kits (Thermo Scientific). Equal amounts of protein samples were combined with NuPAGE™ LDS Sample Buffer (Invitrogen) containing 5% 2-mercaptoethanol (Sigma) and heated at 95 ℃ for 5 minutes. Subsequently, 8-10 μg of each sample was loaded onto SDS-polyacrylamide gels and subjected to electrophoresis until the protein bands were fully separated. Following SDS-PAGE, the proteins were transferred to 0.45 μm polyvinylidene fluoride (PVDF) membranes (Millipore). The PVDF membranes were then blocked with 5% non-fat skim milk for 1 hour at RT. Following blocking, the membranes were incubated overnight at 4℃ with primary antibodies against APP (6E10) (BioLegend), AT180 (Invitrogen), BACE1 (Cell Signaling Technology), Actin (Sigma), and NLRP3 (Cell Signaling Technology). The membranes were then washed with tris-buffered saline with Tween-20 (TBS-T) and incubated with HRP-conjugated anti-mouse or anti-rabbit secondary antibodies (Millipore) for 1 hour at RT. Protein bands were visualized using enhanced chemiluminescence solution (Cytiva) and quantified using ImageJ 1.54f (NIH). All unedited blots and experimental repeats were presented in Supplementary Figure S1 and S2 (*https://www.biosciencetrends.com/action/getSupplementalData.php?ID=233*).

2.16. RNA extraction and real-time quantitative PCR

Total RNA was extracted from brain tissues using RNAiso Plus (Takara) according to the manufacturer's instructions. Equal amounts of RNA were then used to synthesize cDNA with the PrimeScript™ RT Reagent Kit with gDNA Eraser (Takara), following the provided protocol. The synthesized cDNA was diluted 10-fold with RNase-free water. PCR amplification was conducted using TB Green® Premix Ex Taq™ II (Takara) on a CFX Connect (Bio-rad). Relative gene expression was calculated using the housekeeping gene (*Hprt*). The primers used for real-time quantitative PCR were as follows: mouse *Il-1β* forward 5'-agttgacggaccccaaaag-3', mouse *Il-1β* reverse 5'-agctggatgctctcatcagg -3', mouse *Iba1* forward 5'-atctgccgtccaaacttga-3', mouse *Iba1* reverse 5'-ctaggtgggtcttgggaacc-3', mouse *Tnf-α* forward 5'-tcttctcattcctgcttgtgg-3', mouse *Tnf-α* reverse 5'-ggtctgggccatagaactga-3', mouse *Hprt* forward 5'-cctcctcagaccgcttttt-3', and mouse *Hprt* reverse 5'-aacctggttcatcatcgctaa-3'.

2.17. Brain tissue frozen section

Brain tissues preserved in 4% paraformaldehyde were sequentially soaked in 10%, 20%, and 30% sucrose solutions (Junsei), each for one day at 4℃. The tissues were then embedded in FSC 22 Frozen Section Media (Leica) and frozen. The frozen brain samples were sectioned at a thickness of 30 μm using a cryotome (Leica) and stored in a cryoprotectant solution (Biosolution).

2.18. Immunohistochemistry (IHC)

Serially sectioned brain slices were blocked at PBS containing Triton-X 100 solution and 3 % donkey serum (Bio-Rad). Following the blocking step, the slices were incubated overnight at 4 ℃ with the primary antibodies against IBA1 (Wako) and APP (6E10) (BioLegend). On the next day, the slices were washed and incubated with fluorescently labeled secondary antibodies for 1 hour at RT. Subsequently, the slices were washed again and mounted using VECTASHIELD® Antifade Mounting Medium with DAPI (Vector Laboratories). Images were acquired using a confocal microscope (Leica). Analysis of Aβ plaques and IBA1 was performed using the "Surfaces" function in IMARIS software.

2.19. Thioflavin S staining

Brain slices were floated in PBS and stained with 1% thioflavin S (Sigma) dissolved in 50% ethanol for 8 minutes. The tissue samples were then washed with 80 % ethanol twice followed by washing with PBS three times. After washing, the samples were mounted onto slide glass using VECTASHIELD® Antifade Mounting Medium with DAPI (Vector Laboratories).

2.20. RNA sequencing analysis

The procedure was conducted following the previously described method (*21*). Total RNA from mouse cortical tissue was used for mRNA sequencing analysis. Purity and concentration of total RNA were measured using Take 3 (BioTek). RNA integrity was determined using the 2100 Bioanalyzer Instrument (Agilent). Preparation of mRNA library and transcriptome analysis with data quality control was conducted by Novogene Co., LTD (Hong Kong). For quality control, fastq files for all RNA-seq samples were filtered, and the adapters were trimmed. The reads were then aligned to the mouse reference genome GRCm38 by the STAR Aligner. Genes with Fold change > 1.3 and p-value < 0.05 were regarded as differentially expressed.

2.21. Statistical analysis

Graphs were created and statistical analyses were conducted using Prism 8 software (GraphPad Software). Data were analyzed using unpaired two-tailed t-tests, one-way ANOVA with Dunnett's multiple comparisons test, or two-way ANOVA with Dunnett's multiple comparisons test. All data are presented as mean ± standard deviation (SD) or standard error of the mean (SEM). For optical imaging analysis, Origin Pro was utilized for statistical analysis.

2.22. Data Availability

The data that support the findings and materials of this study are available upon request to the corresponding author.

3. Results

3.1. RA-PF reduces BACE1 expression and inflammation in *in vitro* systems.

Among the ramalin derivatives, RA-PF (Figure 1A) demonstrated low toxicity in the Ames test (Figure 1B-C), metabolic stability (Table 1, upper panel), and minimal CYP inhibitory interaction (Table 2, lower panel). It is orally bioavailable (Figure 1D; Table 2, upper panel) and capable of penetrating the blood-brain barrier (Figure 1E; Table 2, lower panel). Previously we demonstrated the BACE1 inhibitory and anti-inflammatory effects of ramalin (*16,17,22*). To evaluate the efficacy of RA-PF on the regulation of BACE1 expression levels in an *in vitro* system, we induced BACE1 under oxidative stress conditions using hydrogen peroxide (H_2O_2) treatment (*23*). H_2O_2 treatment to SH-SY5Y cells, the human neuroblastoma cell line, induced BACE1 expression, while treatment with 5, and 10 μM of RA-PF restored BACE1 expression (Figure 2A, C). We then investigated the effects of RA-PF on neuroinflammation using BV-2, the mouse microglial cell line. Lipopolysaccharide (LPS) treatment induced the NLR family pyrin domain containing 3 (NLRP3) levels and treatment with 10 μM of RA-PF significantly recovered NLRP3 levels (Figure 2B, D).

3.2. Administration of RA-PF restores the synaptic transmission function in primary hippocampal neurons of 5xFAD.

Given ramalin's positive effects in an AD model, we investigated whether RA-PF also possesses therapeutic potential for synaptic dysfunction in an AD model. To monitor synaptic function, particularly synaptic transmission, we employed a pHluorin-based assay. This assay involves pHluorin conjugated to the luminal region of synaptic vesicle membrane proteins such as vesicular glutamate transporter 1 (vGlut1, vG-pH). 10 μM of RA-PF was administered to hippocampal neurons derived from 5xFAD mice. These 5xFAD hippocampal neurons

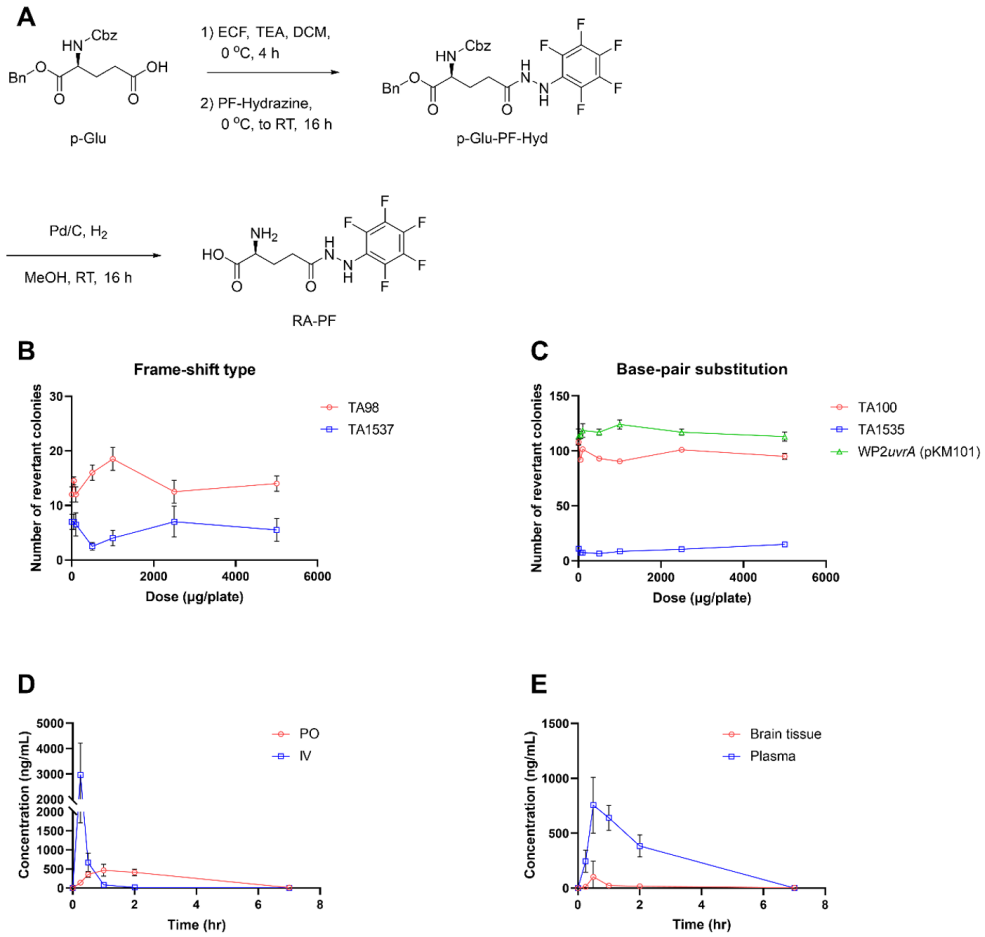

Figure 1. RA-PF has low toxicity and can penetrate the blood-brain barrier via oral administration. (**A**) Scheme showing the synthesis of RA-PF. ECF (Ethyl chloroformate), TEA (Triethyl amine), DCM (Dichloromethane), Pd/C (Palladium on carbon 10 wt. %), MeOH (Methanol), RT (room temperature). (**B** and **C**) Ames test to evaluate the mutagenicity effect of RA-PF. (B) represents frame-shift mutagenicity and (C) represents base-pair substitution mutagenicity. (**D**) Plasma concentration of RA-PF after IV 10 mg/kg and PO 10 mg/kg injection into Sprague-Dawley rats (n = 6). (**E**) Brain tissue and plasma concentration of RA-PF after PO 10mg/kg injection into Sprague-Dawley rats (n = 3).

Table 1. Metabolic stability of RA-PF and CYP inhibitory interaction of RA-PF

Mean remaining (%)				
HLM	MLM	RLM	DLM	MkLM
100.7	99.2	94.4	98.1	100.0
Mean control activity (%)				
CYP1A2	CYP2C9	CYP2C19	CYP2D6	CYP3A
95.2	89.8	88.5	90.7	98.1

HLM: human liver microsomes, MLM: mouse liver microsomes, RLM: rat liver microsomes, DLM: dog liver microsomes, MkLM: monkey liver microsomes.

Table 2. *In vivo* pharmacokinetic parameters of RA-PF

	PO, 10 mg/kg	IV, 10 mg/kg
T_{max} (hr)	1.25 ± 0.612	0.25
C_{max} (ng/mL)	480.320 ± 144.594	2966.155 ± 1251.925
$T_{1/2}$ (hr)	1.062 ± 0.457	1.314 ± 0.251
AUC_{inf} (ng*h/mL)	1279.059 ± 241.783	987.859 ± 358.449
	Plasma	**Brain**	**B/P ratio**
C_{max} (ng/mL)	855.981	105.368	0.123
AUC_{0-7h} (ng*h/mL)	1337.037	111.379	0.083

expressing vG-pH were stimulated with 100 action potentials (AP) at 10 Hz, and fluorescence intensity was measured to quantify synaptic transmission. In wild-type (WT) neurons, the average synaptic transmission following 100 APs was approximately 20%. However, in 5xFAD neurons, synaptic transmission was significantly impaired, decreasing to about 11%. Remarkably, 5xFAD neurons treated with RA-PF exhibited almost complete restoration of synaptic transmission to normal levels (Figure 3A-C), suggesting that RA-PF may have therapeutic effects on synaptic dysfunction in the AD model.

Additionally, we investigated whether RA-PF affects mitochondrial motility, as alterations in mitochondrial trafficking are closely related to AD pathology (*24*). To measure mitochondrial motility, we employed live-cell imaging by introducing Mito-red plasmids into the neurons. In WT neurons, approximately 20% of mitochondria were motile. In contrast, the motility rate in 5xFAD neurons decreased to about 10%. Consistent

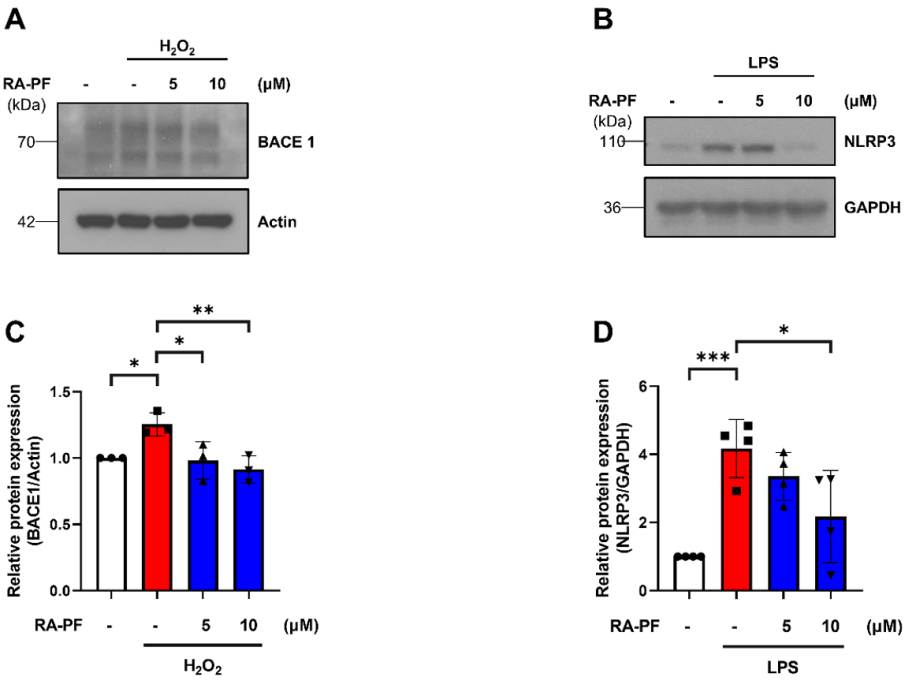

Figure 2. RA-PF ameliorates BACE1 induced by oxidative stress and suppresses LPS-induced inflammatory responses. (**A**) Western blot analysis of BACE1 and Actin following induction with 200 μM of H_2O_2 for 2 hours in SH-SY5Y cells. Cells were pre-treated with RA-PF or vehicle and incubated for 24 hours before H_2O_2 exposure ($n = 3$). (**B**) Western blot analysis of NLRP3 and GAPDH. Cells were treated with RA-PF or vehicle for 24 hours followed by LPS induction for 2 hours ($n = 4$). (**C**) Quantification of BACE1 expression in (A) ($n = 3$). (**D**) Quantification of NLRP3 expression in (B) ($n = 4$). Values are presented as means ± SD. *$p < 0.05$, **$p < 0.01$, and ***$p < 0.001$ versus H_2O_2 or LPS-induced and vehicle pre-treated group; one-way ANOVA with Dunnett's test (C-D).

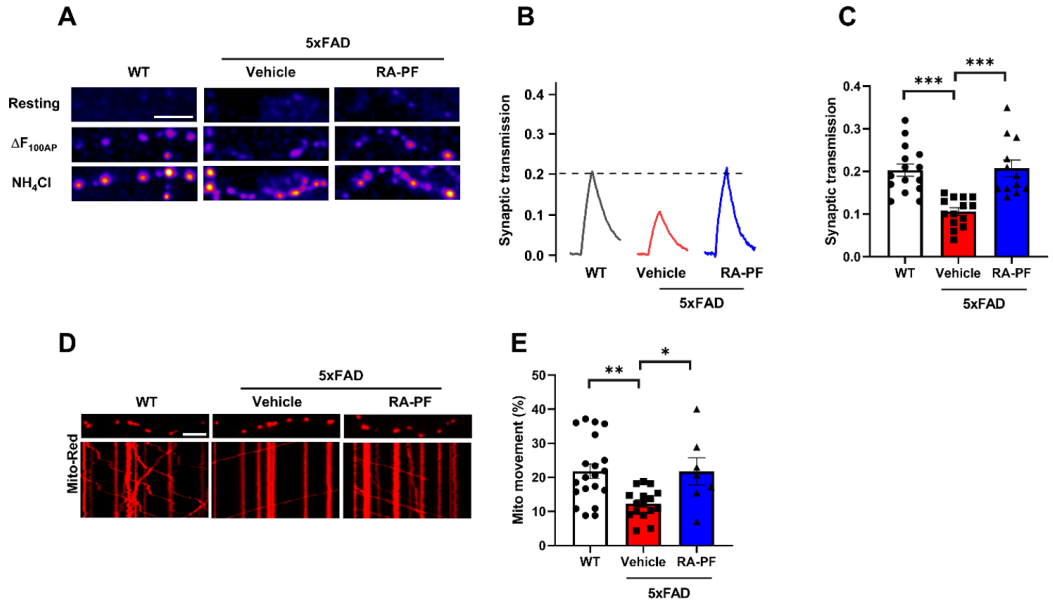

Figure 3. Treatment of RA-PF restores synaptic function and mitochondria movement in 5xFAD hippocampal neurons. (**A**) Representative images of vG-pH at resting (left), 100 AP (middle), and NH_4Cl (right) neurons (Scale bar, 5 mm). (**B**) Representative ensemble average traces of vG-pH in response to 100AP in WT, vehicle treated 5xFAD, and RA-PF treated 5xFAD neurons. Neurons expressed with vG-pH were stimulated at 10Hz 10s with or without RA-PF. Intensities were normalized to the maximal value of NH_4Cl response. (**C**) Mean values of amplitudes of 100AP responses in WT, vehicle treated 5xFAD, and RA-PF-treated 5xFAD neurons. ($n = 12$ - 15). (**D**) Representative image of mitochondria (Top) and its kymograph (Bottom) in WT (left), 5xFAD (middle), and RA-PF-treated 5xFAD (right) neuron (Scale bar, 5 μm). (**E**) Mean values of mitochondria motility rate in WT, 5xFAD, and RA-PF treated 5xFAD neurons. (n = WT: 20, Vehicle treated 5xFAD: 16, RA-PF treated 5xFAD: 7). Values are presented as means ± SEM. *$p < 0.05$, **$p < 0.01$, ***$p < 0.001$ versus vehicle treated 5xFAD group; one-way ANOVA with Dunnett's test (C and E).

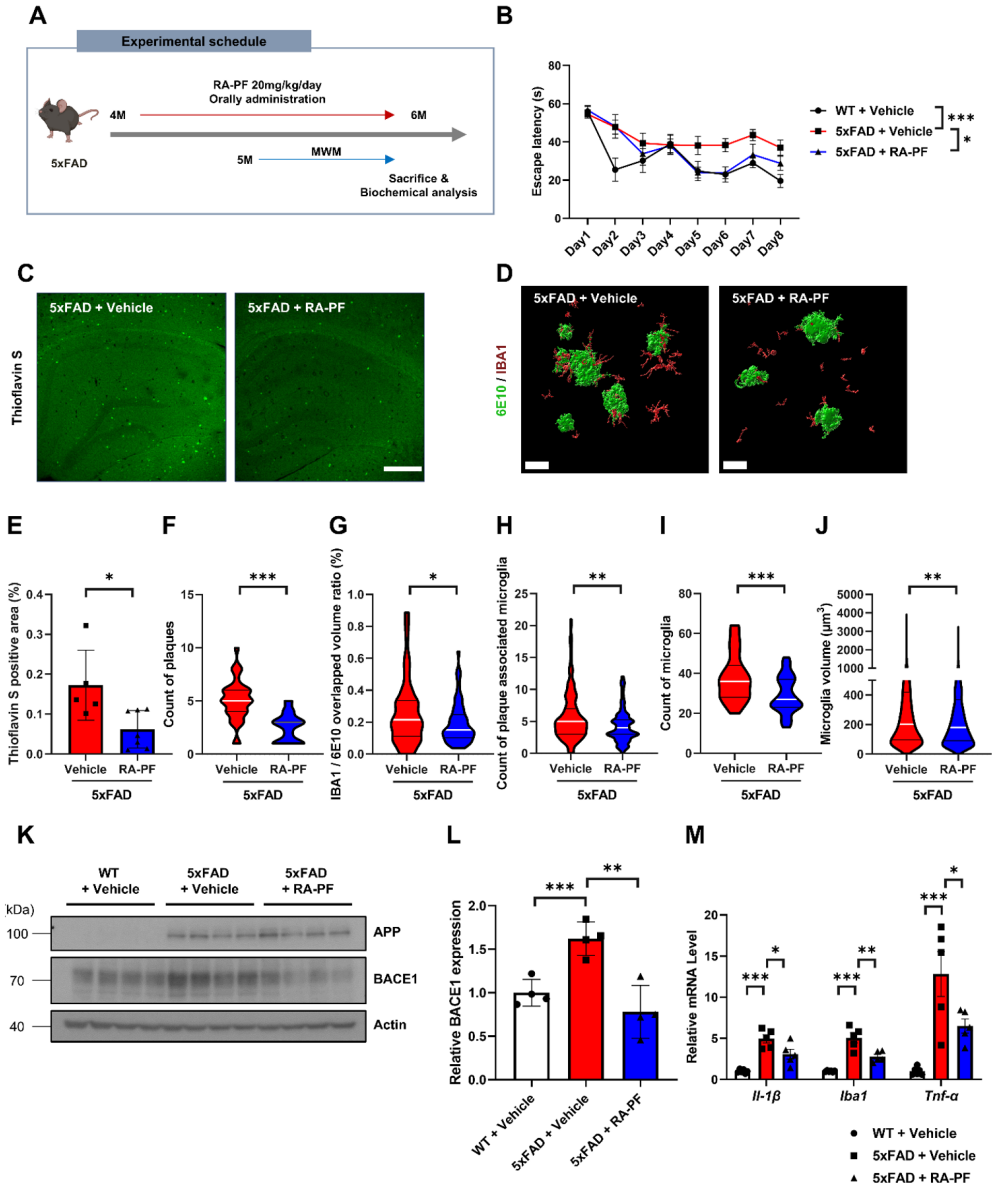

Figure 4. Administration of RA-PF alleviates BACE1 activation, Aβ deposition, inflammatory responses, and cognitive dysfunction in 5xFAD mice. (**A**) A schematic diagram of the experimental design. Created with Biorender.com. (**B**) Escape latency was recorded during the MWM training trials of indicated groups (n = 6 - 12). (**C**) Representative thioflavin S staining images of the hippocampal region. (**D** and **E**) Quantification of thioflavin S positive area (%) in (C) (n = 5 - 7). (**F-J**) IMARIS-based quantification of plaque count in field of view (F) (n = 25 - 34), IBA1 and 6E10 overlapped volume ratio percentage (G) (n = 62 - 172), count of plaque associated microglia (H) (n = 62 - 172), microglial count in field of view (I) (n = 35 - 45), and microgia volume (n = 1309 - 1332) (J) (**K**) Western blot analysis of APP, BACE1, and Actin using the hippocampal samples of 5xFAD (n = 4). (**L**) Quantification of BACE1 expression in (G). (**M**) mRNA expression levels of *Il-1β*, *Iba1*, and *Tnf-α* in the hippocampal samples (n = 6). Values are presented as means ± SEM. *p < 0.05, **p < 0.01, ***p < 0.001, versus 5xFAD + Vehicle; two-way ANOVA with Dunnett's t-test (B), two-tailed Student's t-test (E-J), one-way ANOVA with Dunnett's test (L-M).

with restoring synaptic function, 5xFAD neurons treated with RA-PF showed recovery of mitochondrial motility in the axon (Figure 3D-E). These results collectively suggest that RA-PF positively impacts synaptic function and mitochondrial motility in the AD model, indicating its potential as a therapeutic agent.

3.3. *In vivo* RA-PF administration ameliorates cognitive impairment, BACE1 expression, Aβ plaque deposition, and microglial activation in a 5xFAD mouse model.

To evaluate the therapeutic effects of RA-PF in 5xFAD mice, 20 mg/kg of RA-PF was administrated for 2-month to 4-month-old 5xFAD female mice, followed by behavior study and biochemical analysis at 6 months of age (Figure 4A). As a result, cognitive impairment was observed in the 5xFAD mice in the Morris water maze test, but this impairment was alleviated in the RA-PF administered group (Figure 4B). Additionally, thioflavin S-positive plaques observed in the 5xFAD hippocampus were found to be reduced following

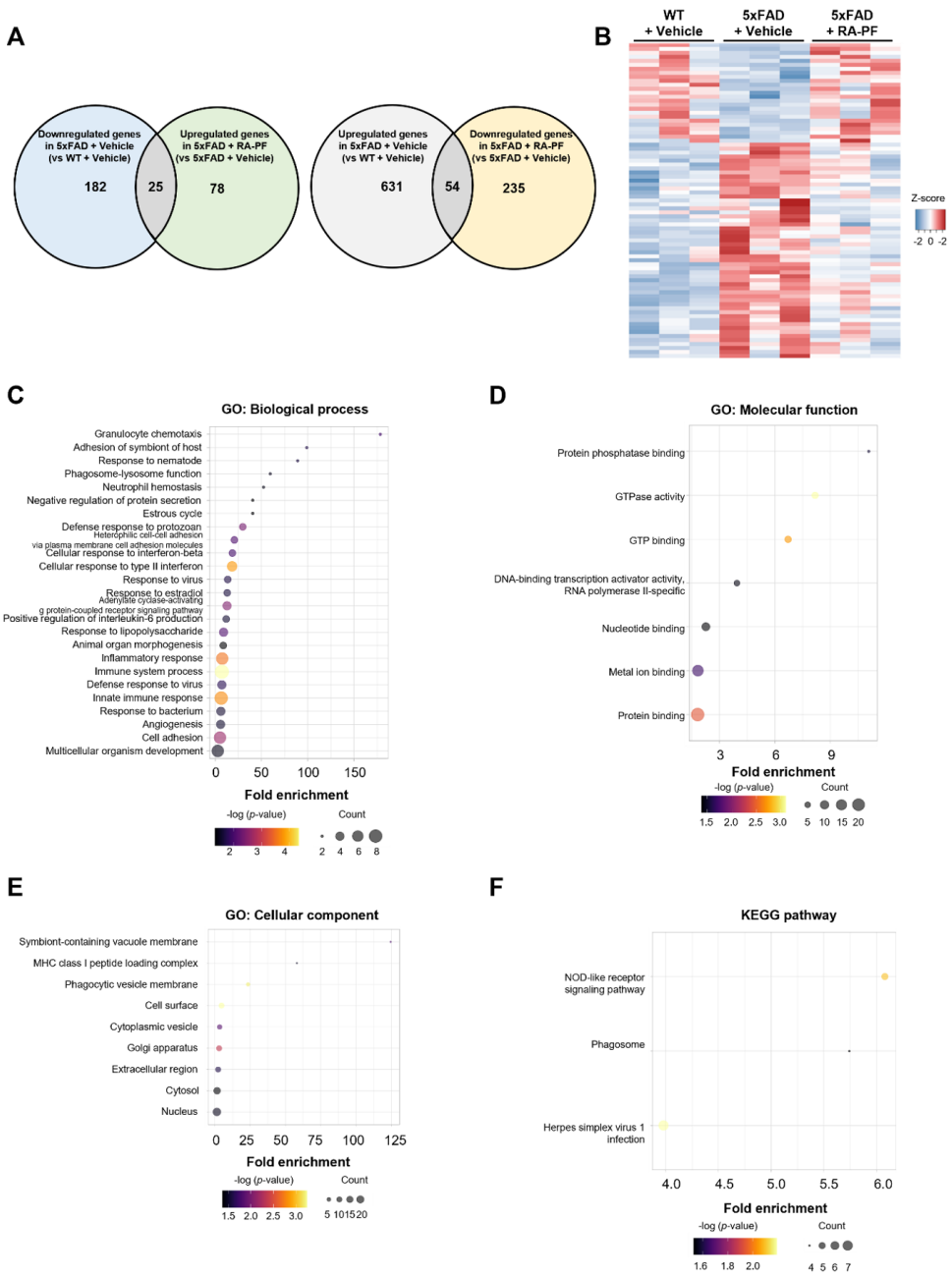

Figure 5. Gene profiling analysis in RA-PF treated 5xFAD mouse model. (**A**) Venn diagrams of DEGs between groups. (**B**) Heatmap panels of 79 DEGs in three groups (WT + Vehicle, 5xFAD + Vehicle, and 5xFAD + RA-PF). (**C**) Gene ontology analysis in biological process category using 79 DEGs. (**D**) Gene ontology analysis in molecular function category using 79 DEGs. (**E**) Gene ontology analysis in cellular component category using 79 DEGs. (**F**) KEGG pathway analysis using 79 DEGs revealed 'NOD-like receptor signaling pathway', 'phagosome', and 'herpes simplex virus 1 infection' pathway-related genes were altered.

RA-PF administration (Figure 4C, E). The 3D image analysis program IMARIS was used to investigate the relationship between Aβ plaque and microglia (Figure 4D). The analysis cross-confirmed that RA-PF treatment reduced the number of plaques (Figure 4F), alongside a decrease in plaque-associated microglia and the overlapped area of 6E10 and IBA1 (Figure 4G-H). Additionally, the number and volume of microglia was significantly reduced (Figure 4I-J). It was also confirmed that the BACE1 upregulation observed in 5xFAD mice was ameliorated by RA-PF treatment (Figure 4K-L) and that the inflammatory response was reduced at the mRNA level of *Il-1β*, *Iba1*, and *Tnf-α* following RA-PF administration (Figure 4M).

3.4. Gene expression profiles following *in vivo* RA-PF administration in 5xFAD mouse model.

To investigate the gene expression changes by RA-PF administration, we conducted the RNA-sequencing using

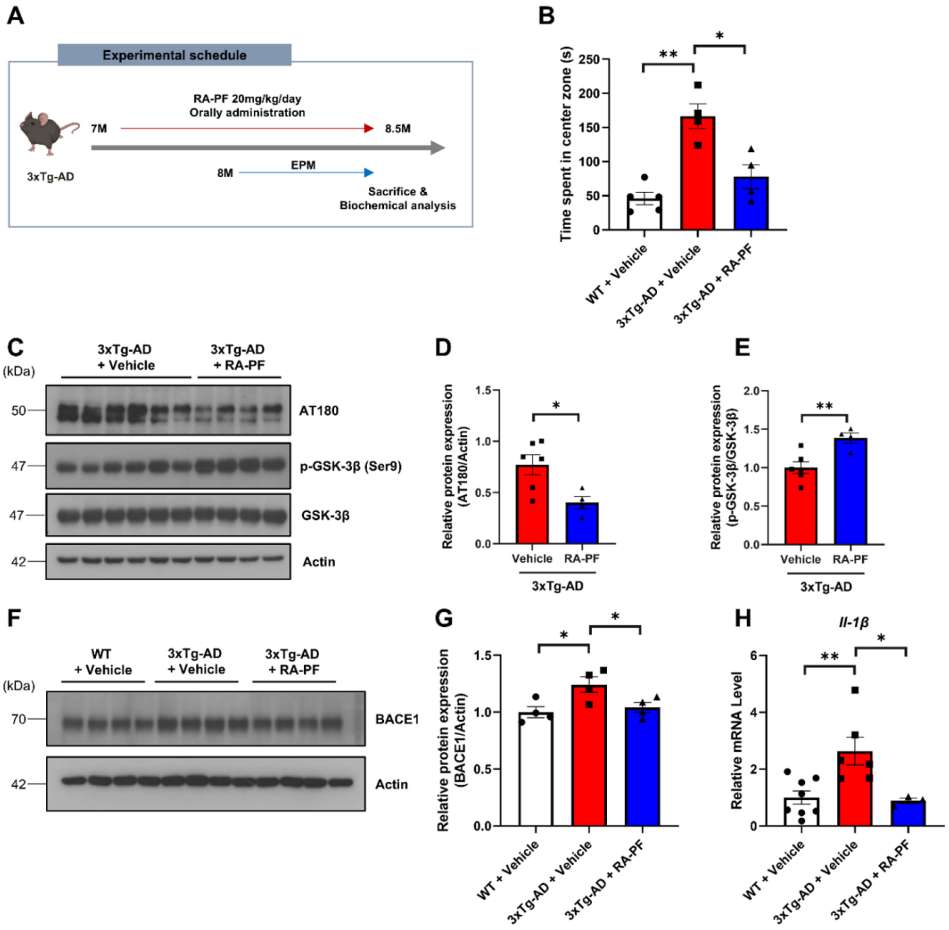

Figure 6. Administration of RA-PF ameliorates BACE1 expression, tau phosphorylation, neuroinflammation, and anxiety in 3xTg-AD mice. (**A**) A schematic diagram of the experimental design. Created with Biorender.com. (**B**) Time spent in the center zone of indicated groups in elevated plus maze test (n = 4 - 6). (**C**) Western blot analysis of AT180 (phospho-Tau Thr231), phospho-GSK-3β Ser9, GSK-3β, and Actin using the cortical samples of indicated groups (n = 4 - 6). (**D-E**) Quantification of AT180 (D) and phospho-GSK-3β Ser9 (E) expression in (C) (n = 4 - 6). (**F**) Western blot analysis of BACE1 and Actin using the cortical samples of indicated groups (n = 4). (**G**) Quantification of BACE1 expression in (E) (n = 4). (**H**) mRNA expression levels of *Il-1β* in the cortical samples of indicated groups (n = 3 - 6). Values are presented as means ± SEM. *p < 0.05 and **p < 0.01, versus 3xTg-AD + Vehicle; two-tailed Student's t-test (D-E), versus 3xTg-AD + Vehicle; one-way ANOVA with Dunnett's test (B, G, and H).

mRNA isolated from the cortice of mice. As a result, there were 25 genes overlapped between downregulated genes in 5xFAD + Vehicle (vs WT + Vehicle) and upregulated genes in 5xFAD + RA-PF (vs 5xFAD + Vehicle) and 54 genes overlapped between upregulated genes in 5xFAD + Vehicle (vs WT + Vehicle) and downregulated genes in 5xFAD + RA-PF (vs 5xFAD + Vehicle) (Figure 5A-B). Gene ontology (GO) analysis using these 79 differentially expressed genes (DEGs) revealed that 'phagosome-lysosome function', 'response to lipopolysaccharide', and 'inflammatory response'-related genes were significantly enriched in biological process (Figure 5C). In the molecular function category, 'protein phosphatase binding', 'nucleotide binding', and 'protein binding'-related genes were enriched and 'phagocytic vesicle membrane', 'cytoplasmic vesicle', and 'nucleus'-related genes were enriched in cellular component category (Figure 5D-E). Kyoto Encyclopedia of Genes and Genomes (KEGG) pathway analysis revealed that significant enrichment in 'NOD-like receptor signaling pathway', 'phagosome', and 'herpes simplex virus 1 infection' pathway (Figure 5F).

3.5. *In vivo* RA-PF administration ameliorates BACE1 expression, tau phosphorylation, and anxiety in 3xTg-AD mouse model.

To further investigate the effects of RA-PF on AD, we orally administered 20 mg/kg of RA-PF to 7-month-old 3xTg-AD, a widely used AD model (Figure 6A). In the elevated plus maze test, 3xTg-AD mice spent more time in the center zone than other groups and RA-PF administration significantly recovered time spent in the center zone compared to 3xTg-AD + Vehicle (Figure 6B). Biochemical analysis revealed a significant reduction in tau phosphorylation following RA-PF administration (Figure 6C-D). GSK-3β is a key regulator of tau phosphorylation at the Thr231 site (*25*), and its inactive form, phosphorylated GSK-3β at the Ser9 site, was upregulated following RA-PF treated group

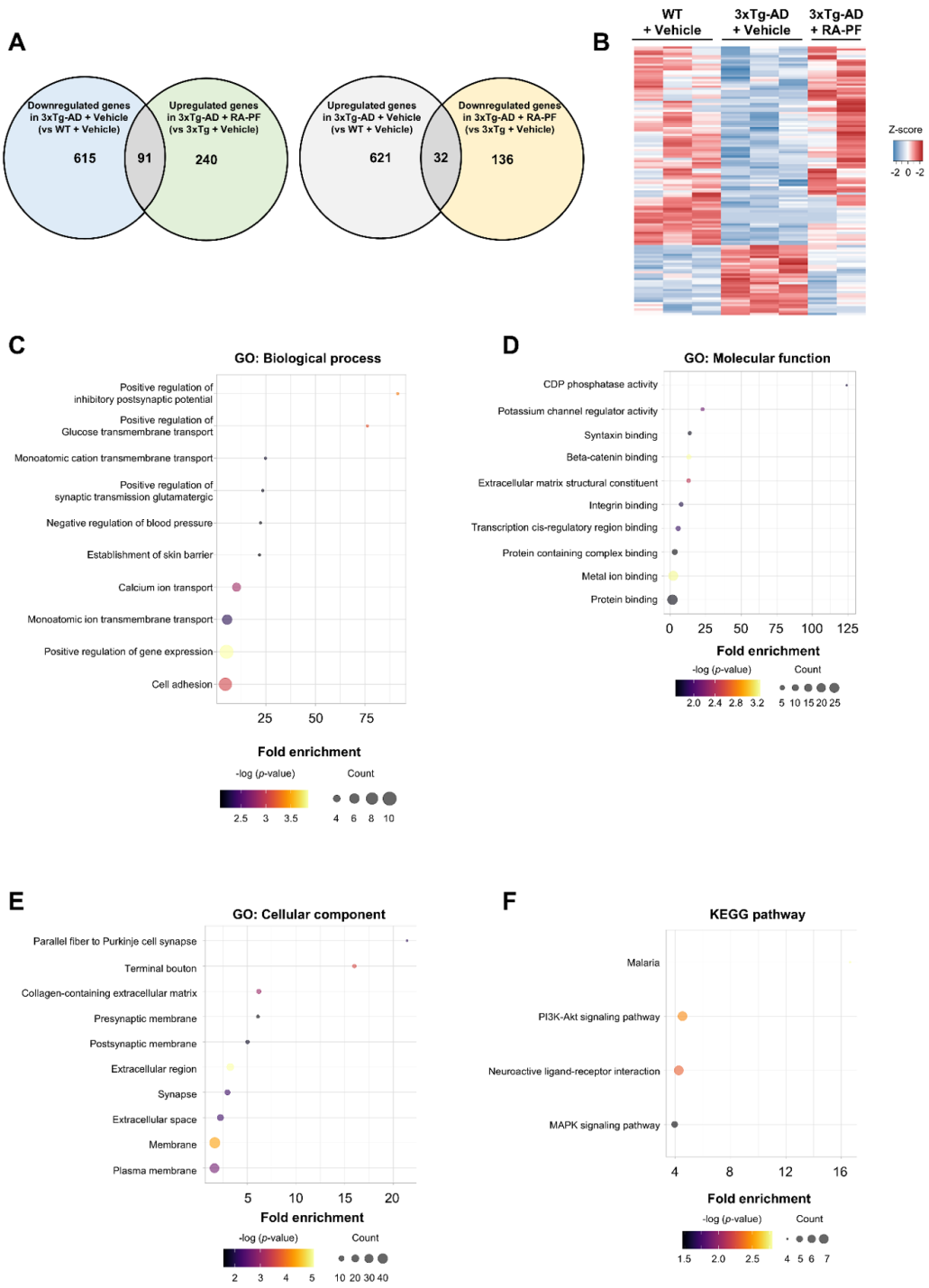

Figure 7. Gene profiling analysis in RA-PF treated 3xTg-AD mice. (**A**) Venn diagrams of DEGs between groups. (**B**) Heatmap panels of 123 DEGs in three groups (WT + Vehicle, 3xTg-AD + Vehicle, and 3xTg-AD + RA-PF). (**C**) Gene ontology analysis in biological process category using 123 DEGs. (**D**) Gene ontology analysis in molecular function category using 123 DEGs. (**E**) Gene ontology analysis in cellular component category using 123 DEGs. (**F**) KEGG pathway analysis using 123 DEGs revealed 'malaria', 'PI3K-Akt signaling pathway', 'neuroactive ligand-receptor interaction', and 'MAPK signaling pathway'-related genes were altered.

(Figure 6C, E). Additionally, BACE1 expression in 3xTg-AD mice also recovered (Figure 6F-G) and the neuroinflammation marker, *Il-1β* was reduced at the mRNA level after RA-PF treatment (Figure 6H).

3.6. Gene expression profiles following RA-PF *in vivo* administration in the 3xTg-AD mouse model.

To examine RA-PF efficacy on 3xTg-AD, we further evaluated the gene expression profile of the cortical region. 91 genes were overlapped between downregulated genes in 3xTg-AD + Vehicle (vs WT + Vehicle) and upregulated genes in 3xTg + RA-PF (vs 3xTg-AD + Vehicle), and 32 genes were overlapped between upregulated genes in 3xTg-AD + Vehicle (vs

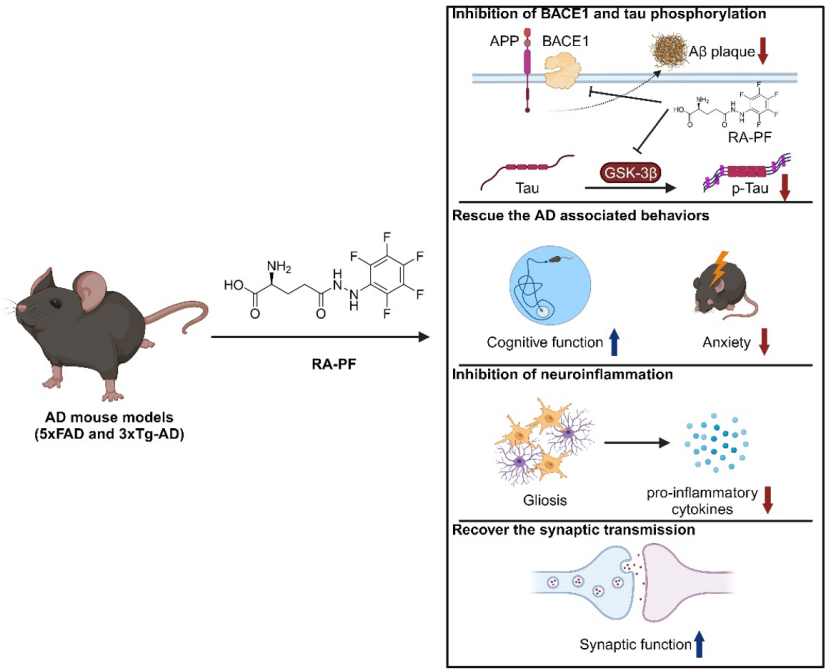

Figure 8. Schematic illustration of RA-PF's therapeutic effect of RA-PF on AD mouse models. Orally administered RA-PF crosses the blood-brain barrier and reduces Aβ plaques by BACE1 inhibition, alongside decreasing tau phosphorylation *via* GSK-3β inactivation. Additionally, RA-PF alleviates neuroinflammation and enhances synaptic transmission. These effects improve AD-associated behaviors, including cognitive function and anxiety. Created with Biorender.com.

WT + Vehicle) and downregulated genes in 3xTg-AD + RA-PF (vs 3xTg + Vehicle) (Figure 7A-B). Using these 123 DEGs, we further analyzed functional annotations and found that 'positive regulation of inhibitory postsynaptic potential', 'positive regulation of synaptic transmission glutamatergic', and 'calcium ion transport'-related genes were significantly enriched in biological process (Figure 7C). 'Potassium channel regulator activity', 'syntaxin binding', and 'protein binding' were enriched in molecular function category (Figure 7D) and we further identified significant enrichment in 'presynaptic membrane', 'postsynaptic membrane' and 'synapse' in cellular component category (Figure 7E). KEGG pathway analysis revealed that 'PI3K-Akt signaling pathway', 'neuroactive ligand-receptor interaction', and 'MAPK signaling pathway' were significantly enriched (Figure 7F).

4. Discussion

This study highlights the therapeutic potential of RA-PF in modulating AD pathogenesis. While the therapeutic potential of ramalin and its derivatives for AD has been proposed (*17,22*), their *in vivo* efficacy has not yet been reported. To enhance the therapeutic potential of ramalin, we designed and synthesized several derivatives by substituting its phenyl ring with different structural groups. Among them, RA-PF was identified through toxicity screening as having the lowest *in vivo* toxicity, being orally bioavailable, and capable of penetrating the blood-brain barrier (Figure 1B-E; Table 1-2). Our results demonstrate that RA-PF significantly reduces BACE1 expression and neuroinflammation in the AD models. Targeting BACE1 has long been proposed as a therapeutic approach for AD. However, many studies have failed because BACE1 has numerous binding partners and full BACE1 inhibitors have been unsuccessful in drug development due to toxicity (*26*). Nevertheless, BACE1 remains an attractive target for AD therapy, and new approaches to its inhibition are being explored, including partial BACE1 inhibitors and indirect BACE1 regulators (*10,11*). These alternatives offer safety advantages over full BACE1 inhibitors or BACE1 knockout approaches while effectively reducing Aβ plaque deposition. In this context, it restores BACE1 levels to normal under various AD conditions, leading to cognitive improvement and reduced plaque deposition.

In AD condition, microglia become hyperactivated around Aβ plaques leading to neuroinflammation. Our RNA-seq data revealed that terms related to phagocytosis, such as 'phagosome-lysosome function' (Figure 5C), 'phagocytic vesicle membrane' (Figure 5E), and 'phagosome' (Figure 5F) were dysregulated in 5xFAD group, while effectively normalized by RA-PF administration. Based on these findings, we focused on the relationship between plaques and microglia. Microglial activation (*27*) and plaque-associated microglia observed in 5xFAD were mitigated by RA-PF treatment (Figure 4G-J), which was associated

with neuroinflammation (Figure 4M). Paradoxically, this process also resulted in a reduction in Aβ plaque levels (Figure 4E-F), which we interpret as a complex phenomenon mediated by RA-PF's regulation of BACE1 (Figure 4K-L). To further evaluate the impact of RA-PF beyond the regulation of BACE1 and neuroinflammation, we utilized the 3xTg-AD model to investigate its effects on tau. In this model, RA-PF administration reduced tau phosphorylation, accompanied by the suppression of GSK-3β activity, a key regulator of tau hyperphosphorylation (Figure 6C-E). AD pathogenesis does not follow a single specific pathogenesis. It involves multiple pathogenic processes, including the accumulation of misfolded proteins, neuroinflammation, and mitochondrial dysfunction. Targeting these multiple processes is advantageous for treating diseases with complex pathogenesis (*28,29*). RA-PF not only regulates BACE1 expression but also inhibits neuroinflammation, and tau phosphorylation and restores synaptic function making it a more effective treatment for AD.

In conclusion, this study demonstrated that RA-PF targets multiple aspects of AD pathogenesis. The findings highlight the potential of RA-PF as a therapeutic agent addressing the complex pathologies involved in AD progression, introducing a novel compound for AD treatment (Figure 8). However, it remains unclear how RA-PF regulates BACE1 expression, ameliorates neuroinflammation, and restores synaptic functions. Further studies are needed to elucidate the detailed mechanism underlying these effects. Moreover, this study is based on pre-clinical models, it remains uncertain whether the observed effects will translate effectively to clinical settings. For clinical application, a comprehensive risk-benefit assessment will be essential.

Funding: This work was supported by Korea Institute of Marine Science & Technology Promotion (KIMST) grant funded by the Ministry of Oceans and Fisheries (RS-2021-KS211513).

Conflict of Interest: Kim H and Park SY are employees of Ahngook Pharmaceutical Co.. The other authors have no conflicts of interest in this work.

References

1. Cho Y, Bae HG, Okun E, Arumugam TV, Jo DG. Physiology and pharmacology of amyloid precursor protein. Pharmacol Ther. 2022; 235:108122.
2. Deng Y, Wang H, Gu K, Song P. Alzheimer's disease with frailty: Prevalence, screening, assessment, intervention strategies and challenges. Biosci Trends. 2023; 17:283-292.
3. Peng Y, Song P, Karako T, Asakawa T. Blocking progression from intervenable mild cognitive impairment to irreversible dementia, what can we do? Biosci Trends. 2024; 18:409-412.
4. Park J, Lai MKP, Arumugam TV, Jo DG. O-GlcNAcylation as a therapeutic target for Alzheimer's disease. Neuromolecular Med. 2020; 22:171-193.
5. Ma YN, Hu X, Karako K, Song P, Tang W, Xia Y. Exploring the multiple therapeutic mechanisms and challenges of mesenchymal stem cell-derived exosomes in Alzheimer's disease. Biosci Trends. 2024.
6. Hong S, Baek S-H, Lai MKP, Arumugam TV, Jo D-G. Aging-associated sensory decline and Alzheimer's disease. Molecular Neurodegeneration. 2024; 19:93.
7. Vassar R. BACE1 inhibitor drugs in clinical trials for Alzheimer's disease. Alzheimers Res Ther. 2014; 6:89.
8. Ghosh AK, Brindisi M, Tang J. Developing β-secretase inhibitors for treatment of Alzheimer's disease. J Neurochem. 2012; 120 Suppl 1:71-83.
9. Ugbaja SC, Lawal IA, Abubakar BH, Mushebenge AG, Lawal MM, Kumalo HM. Allostery inhibition of BACE1 by psychotic and meroterpenoid drugs in Alzheimer's disease therapy. Molecules. 2022; 27:4372.
10. Bahn G, Park J-S, Yun UJ, *et al*. NRF2/ARE pathway negatively regulates BACE1 expression and ameliorates cognitive deficits in mouse Alzheimer's models. Proc Natl Acad Sci U S A. 2019; 116:12516-12523.
11. Han J, Sul JH, Lee J, Kim E, Kim HK, Chae M, Lim J, Kim J, Kim C, Kim JS, Cho Y, Park JH, Cho YW, Jo DG. Engineered exosomes with a photoinducible protein delivery system enable CRISPR-Cas-based epigenome editing in Alzheimer's disease. Sci Transl Med. 2024; 16:eadi4830.
12. Leng F, Edison P. Neuroinflammation and microglial activation in Alzheimer disease: Where do we go from here? Nat Rev Neurol. 2021; 17:157-172.
13. Hu X, Ma YN, Xia Y. Association between abnormal lipid metabolism and Alzheimer's disease: New research has revealed significant findings on the APOE4 genotype in microglia. Biosci Trends. 2024; 18:195-197.
14. Larson KC, Martens LH, Marconi M, Dejesus C, Bruhn S, Miller TA, Tate B, Levenson JM. Preclinical translational platform of neuroinflammatory disease biology relevant to neurodegenerative disease. J Neuroinflammation. 2024; 21:37.
15. Gao C, Jiang J, Tan Y, Chen S. Microglia in neurodegenerative diseases: Mechanism and potential therapeutic targets. Signal Transduct Target Ther. 2023; 8:359.
16. Paudel B, Bhattarai HD, Koh HY, Lee SG, Han SJ, Lee HK, Oh H, Shin HW, Yim JH. Ramalin, a novel nontoxic antioxidant compound from the Antarctic lichen Ramalina terebrata. Phytomedicine. 2011; 18:1285-1290.
17. Kim TK, Cho Y, Kim J, Lee J, Hong JM, Cho H, Kim JS, Lee Y, Kim KH, Kim IC, Han SJ, Oh H, Jo DG, Yim JH. Synthesis and evaluation of chloride-substituted ramalin derivatives for Alzheimer's disease treatment. Molecules. 2024; 29:3701.
18. Park J, Ha H-J, Chung ES, *et al*. O-GlcNAcylation ameliorates the pathological manifestations of Alzheimer's disease by inhibiting necroptosis. Sci Adv. 2021; 7:eabd3207.
19. Walf AA, Frye CA. The use of the elevated plus maze as an assay of anxiety-related behavior in rodents. Nat Protoc. 2007; 2:322-328.
20. Bae JR, Lee W, Jo YO, Han S, Koh S, Song WK, Kim SH. Distinct synaptic vesicle recycling in inhibitory nerve terminals is coordinated by SV2A. Prog Neurobiol. 2020; 194:101879.
21. Kim J-S, Jun JH, Lee J, *et al*. HDAC6 mediates NLRP3 inflammasome activation in the pathogenesis of diabetic

retinopathy. Metabolism. 2024; 164:156108.
22. Kim TK, Hong JM, Kim KH, Han SJ, Kim IC, Oh H, Yim JH. Potential of ramalin and its derivatives for the treatment of Alzheimer's disease. Molecules. 2021; 26:6445.
23. Mouton-Liger F, Paquet C, Dumurgier J, Bouras C, Pradier L, Gray F, Hugon J. Oxidative stress increases BACE1 protein levels through activation of the PKR-eIF2α pathway. Biochim Biophys Acta. 2012; 1822:885-896.
24. Correia SC, Perry G, Moreira PI. Mitochondrial traffic jams in Alzheimer's disease - pinpointing the roadblocks. Biochim Biophys Acta. 2016; 1862:1909-1917.
25. Cho JH, Johnson GV. Primed phosphorylation of tau at Thr231 by glycogen synthase kinase 3β (GSK3beta) plays a critical role in regulating tau's ability to bind and stabilize microtubules. J Neurochem. 2004; 88:349-358.
26. Mullard A. BACE failures lower AD expectations, again. Nat Rev Drug Discov. 2018; 17:385.
27. Chan TE, Grossman YS, Bloss EB, Janssen WG, Lou W, McEwen BS, Dumitriu D, Morrison JH. Cell-type specific changes in glial morphology and glucocorticoid expression during stress and aging in the medial prefrontal cortex. Front Aging Neurosci. 2018; 10:146.
28. Gong CX, Dai CL, Liu F, Iqbal K. Multi-targets: An unconventional drug development Strategy for Alzheimer's disease. Front Aging Neurosci. 2022; 14:837649.
29. Jun JH, Kim JS, Palomera LF, Jo DG. Dysregulation of histone deacetylases in ocular diseases. Arch Pharm Res. 2024; 47:20-39.

Received November 11, 2024; Revised December 30, 2024; Accepted January 22, 2025.

[§]These authors contributed equally to this work.

*Address correspondence to:
Joung Han Yim, Division of Polar Life Sciences, Korea Polar Research Institute, Incheon 21990, Korea.
E-mail: jhyim@kopri.re.kr

Dong-Gyu Jo, School of Pharmacy, Sungkyunkwan University, Suwon 16419, Korea.
E-mail: jodg@skku.edu

Released online in J-STAGE as advance publication January 25, 2025.